

doi:10.15199/48.2018.04.02

Temperature and frequency dependent Preisach model

Abstract. The present paper deals with a frequency and temperature dependent modeling approach for hysteresis loops of ferromagnetic materials. The model is based on the Preisach model. The frequency dependency is taken into account by the statistical loss theorem, while thermal effects were incorporated by a generalization of the model equation. The model was validated against measurements made on a soft magnetic material. The results of the proposed model were in good agreement with measured data.

Streszczenie. W artykule zaprezentowano modelowanie pętli histerezy materiałów ferromagnetycznych uwzględniające wpływ temperatury i częstotliwości a bazujące na modelu Preisacha. Wpływ częstotliwości uwzględniał teorię strat. **Rozszerzenie modelu Preisacha uwzględniające wpływ temperatury i częstotliwości.**

Keywords: frequency-dependent hysteresis, temperature-dependent hysteresis, Preisach modelin

Słowa kluczowe: model Preisacha, Modelowanie materiałów magnetycznychh, wpływ temperatury, wpływ częstotliwości

Introduction

Ferromagnetic hysteresis is present in the operation of most electrical engineering equipments, e.g. electric motors, transformers, components for power electronics and so on. The phenomena occurs power losses in these devices that must be taken into account during the design phase. Accurate power prediction can only be performed by accurate models. Preisach modeling and Jiles–Atherton techniques are the most fruitful techniques to take hysteresis into account [1, 2, 3, 4, 5, 6, 7, 8, 9, 10, 11, 12].

In this paper, taking the temperature effects into consideration at different frequency of the source field is presented. Measured hysteresis loops depending on the frequency and the temperature are shown and compared with the identified extended Preisach model.

The measurement system

The detailed description of the measurement system can be found in [13, 14]. Here a short presentation is given. The block diagram of the developed measurement system is shown in Fig. 1. Fig. 2 presents a photograph about the setup. Hysteresis characteristics have been measured using a toroidal shape core made of laminated soft magnetic material (M250-35A manufactured by the ArcerolMittal company).

The magnetic field inside the specimen has been generated by the current $i(t)$ flowing in the primary coil with $N_p = 94$ turns. The arbitrary waveform of current has been generated by LabVIEW functions. The time variation of the magnetic field intensity results in a time varying magnetic flux $\Phi(t)$ inside the specimen, finally the effect of this flux can be measured by the secondary coil wound on the core. The secondary coil has $N_s = 121$ turns which output is the induced voltage $u(t)$.

The magnetic field intensity is calculated from the current of the primary coil:

$$(1) \quad H(t) = \frac{N_p i(t)}{l},$$

where $l = 163\text{mm}$ is the mean length of the core. The magnetic flux density is obtained from the induced voltage of the secondary coil:

$$(2) \quad B(t) = B_0 + \frac{1}{SN_s} \int_0^t u(\tau) d\tau,$$

where $S = 26.25\text{mm}^2$ is the cross section of the specimen. It is noted that 15 laminates have been glued to prepare the

core. The thickness of one lamination is 0.35mm , inner and outer radii of the toroid are 24mm and 29mm . Finally, the constant B_0 is the DC component of the measured periodic flux density.

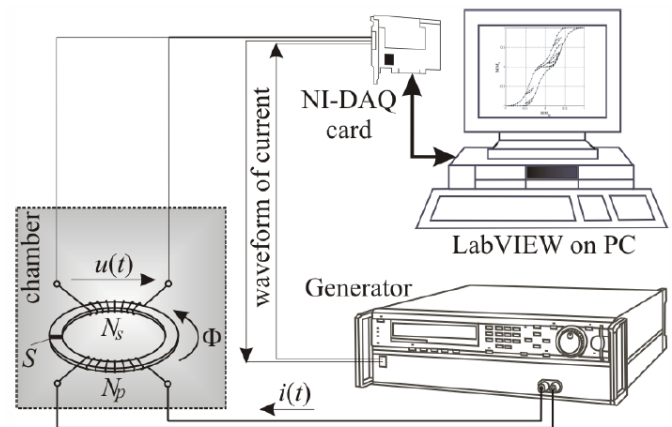


Fig. 1. Block diagram of the measurement system

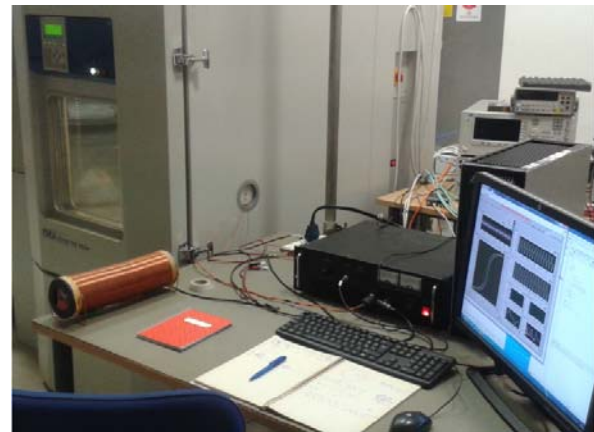


Fig. 2. The measurement system in the laboratory

The waveform generation, the measurements and postprocessing of measured signals have been worked out by using LabVIEW functions. A National Instruments Data Acquisition Card (NI-DAQ) PCI-6251 has been used for current generation and picking up measured data. The current generator is a voltage controlled current generator which output current is proportional to the controlling voltage.

The specimen has been inserted into a chamber to control the temperature.

Measurements have been performed in the range of $T = 20\text{ }^{\circ}\text{C}, \dots, 660\text{ }^{\circ}\text{C}$, and between $f = 5\text{ Hz}$ and $f = 200\text{ Hz}$. Instrumental uncertainty has been found above $T = 500\text{ }^{\circ}\text{C}$, the upper limit has been set to this value. Both the frequency and temperature dependency of the hysteresis loops have been studied comprehensively.

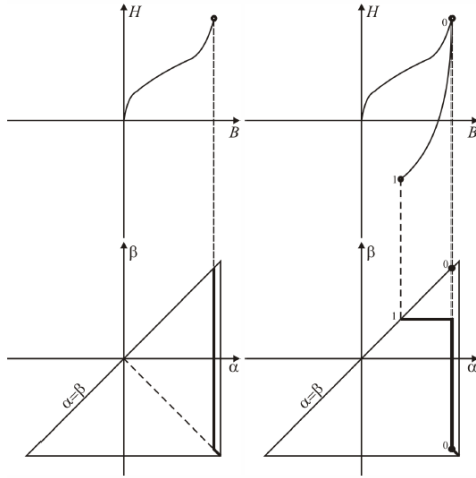


Fig. 3. The first and second step

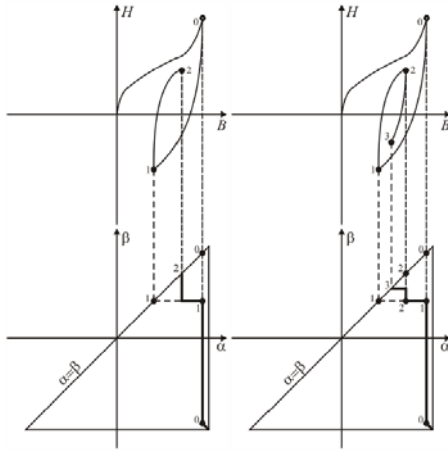


Fig. 4. The third and fourth step

The static Preisach model

The classical Preisach model [15, 16, 17, 18, 19] has been implemented to approximate the static hysteresis characteristics applying the inverse style, i.e. the input and the output of the model are the magnetic flux density and the magnetic field intensity, respectively. The Everett function $E(\alpha, \beta)$ has been identified instead of the probability function to speed up the model.

The staircase line is stored and managed in a special way to decrease to the memory consumption, because the model is planned to insert into numerical electromagnetic field analysis. The model is working as presented in the following four steps.

By increasing the magnetic flux density from demagnetized state, the magnetic field intensity is increasing according to the first magnetization curve, and the staircase line is moving from left to right (Fig. 3).

Fig. 3 illustrates the situation when the magnetic flux as well as the magnetic field is decreasing along a concentric minor loop. The staircase line is moving from up to down. The point 0 is stored in the memory of the model: $L = \{\alpha_0\}$. Only the value of α is stored. The output of the model is obtained by:

$$(3) H(t) = H_{\max} \left(-E(\alpha_0, \beta_0) + 2 \left[E(\alpha_1, \beta_0) - E(\alpha_1, \beta_1) \right] \right),$$

where $\beta_0 = -\alpha_0$ from the list of L , moreover $\alpha_1 = \alpha_0$ and $\beta_1 = B(t)/B_{\text{sat}}$. The input and output are normalized by the magnetic flux density at saturation B_{sat} and the corresponding magnetic flux density H_{\max} , respectively.

The input is increasing according to Fig. 4 (see point 1) resulting a minor loop. A part of the staircase line is moving from left to right and a new staircase is appearing, i.e. a new point is stored in the memory: $L = \{\beta_1, \alpha_0\}$. The output of the model is calculated as

$$(4) H(t) = H_{\max} \left(-E(\alpha_0, \beta_0) + 2 \left[E(\alpha_1, \beta_0) - E(\alpha_1, \beta_1) + E(\alpha_2, \beta_1) - E(\alpha_2, \beta_2) \right] \right),$$

Here $\alpha_2 = B(t)/B_{\text{sat}}$

The situation according to a higher order minor loop can be seen in Fig. 4 with the state: $L = \{\beta_1, \alpha_2, \alpha_0\}$.

Fig. 5 shows higher order minor loops generated by the model. The curves are agree well with measurements.

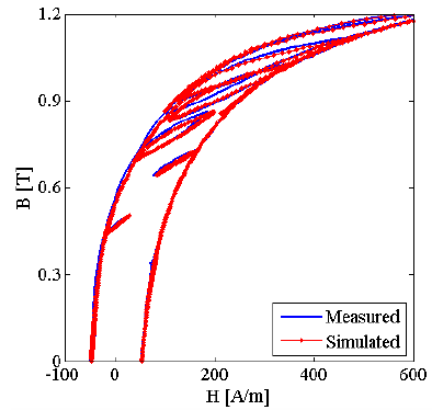


Fig. 5. Higher order minor loops at 5Hz

Frequency dependent Preisach model

According to the statistical loss separation theorem, the magnetic field intensity $H(t)$ is divided into three parts [16, 17, 18, 19]:

$$(5) H(t) = H_{st}(B(t)) + H_{eddy}(B(t), \dot{B}(t)) + H_{exc}(B(t), \dot{B}(t)),$$

where $H_{st}(B(t))$ is the static term given by the aforementioned static Preisach model. This term is independent of the frequency. The second term is occurred by the eddy current field inside the lamination, and finally, the third magnetic field intensity term is according to the excess losses caused by micro-eddy currents.

The decomposed magnetic field intensity has the following form [16, 17, 18, 19]:

$$(6) H(t) = H_{st}(B(t)) + \frac{\sigma d^2}{12} \delta \left| \frac{dB}{dt} \right|^\gamma + \delta \left| \frac{1}{R} \frac{dB}{dt} \right|^{1/\nu}$$

with $\delta = \text{sign}(dB/dt)$. The conductivity and thickness of the lamina under study are denoted by σ and d . The term $\sigma d^2/12$ is constant and valid only if the magnetic flux density is sinusoidal in time and homogeneous inside the lamination. In general case this is not true. The effect of nonlinear behavior of the classical eddy current on the magnetic field intensity can be taken into account by the exponent γ with the following formula [18, 19]:

$$(7) \gamma = \gamma(B(t)) = a_0 + a_1 \delta \frac{B(t)}{B_{\text{sat}}} + a_2 \left(\frac{B(t)}{B_{\text{sat}}} \right)^2,$$

where B_{sat} is the magnetic flux density value at technical saturation, a_0 , a_1 and a_2 are model parameters. The function of R has been selected as [16, 17]

$$(8) \quad R = R(B(t)) = \frac{R_0}{1 - \left(\frac{B(t)}{B_{sat}}\right)^2},$$

where R_0 is a constant value as well as v .

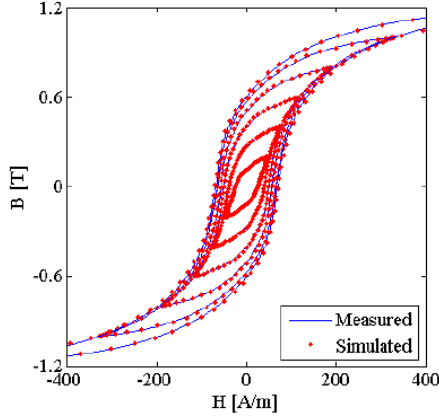


Fig. 6. Dynamic hysteresis loops measured and simulated at 50Hz

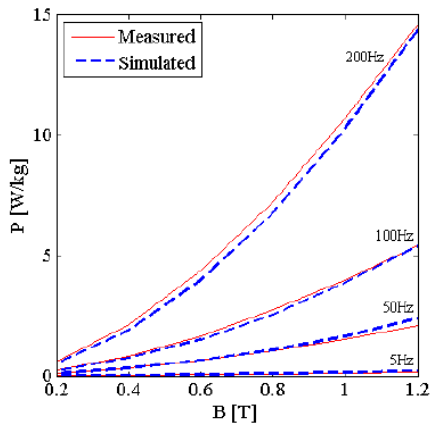


Fig. 7. Measured and simulated losses

The parameters a_0 , a_1 , a_2 , R_0 and v are identified from dynamic hysteresis loops measured at 5Hz, 50Hz, 100Hz and 200Hz. The following parameters have been found to give an adequate approximation:

$$a_0 = 1.1144, a_1 = 0.0071, a_2 = -0.1294, R_0 = 24.305, v = 1.5194.$$

A comparison between measured and simulated concentric minor loops is shown in Fig. 6. Fig. 7 shows a comparison between measured and simulated losses, i.e. the area of the hysteresis loop.

The extended model

The frequency dependent model has been generalized to take the temperature T into account. The static term is independent from the frequency, but it is depending on the temperature. The eddy current field as well as the excess field have been modified, too, i.e.

$$(9) \quad H(t) = H_{st}(B(t), T) + H_{eddy}(B(t), \dot{B}(t), T) + H_{exc}(B(t), \dot{B}(t), T)$$

The following expression has been developed:

$$(10) \quad H(t) = H_{st}(B(t), T) + \frac{\sigma d^2}{12} \delta \left| \frac{dB}{dt} \right|^\gamma + \frac{\delta}{1 - e^{-\frac{T_C - T}{\beta_1}}} + \frac{\delta}{1 - e^{-\frac{T_C - T}{\beta_2}}} \left| \frac{1}{R} \frac{dB}{dt} \right|^{1/\nu}.$$

Three new parameters have been introduced: T_C , β_1 and β_2 .

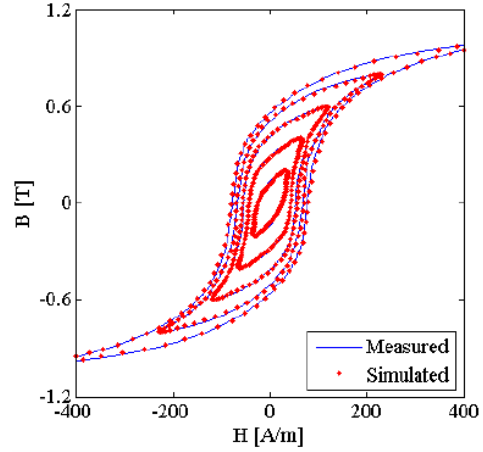


Fig. 8. Hysteresis loops at 420°C and 50Hz

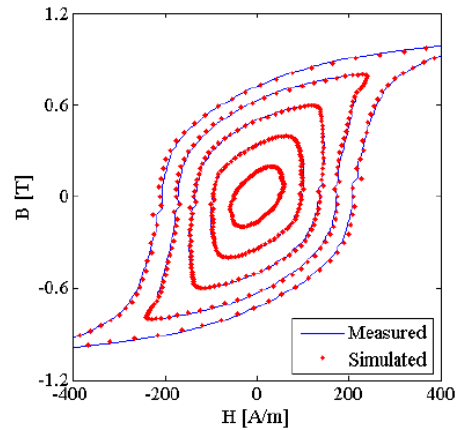


Fig. 9. Hysteresis loops at 420°C and 200Hz

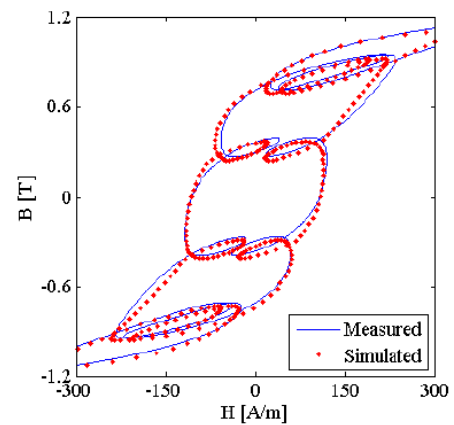


Fig. 10. Higher order minor loops at 100°C and 100Hz

The following parameters have been found to give an adequate approximation:

$$a_0 = 1.0693, a_1 = 0.0021, a_2 = -0.1211, R_0 = 109.6203, v = 1.569, \beta_1 = 365.1020, \beta_2 = 467.5795, T_C = 539.8476.$$

Fig. 8, Fig. 9 and Fig. 10 present comparisons between measured and simulated hysteresis loops at higher temperate and different frequency.

The three terms of loss have been determined, too, at different temperature levels. Losses are increasing by increasing the temperature, as it can be seen in Fig. 11 and Fig. 12.

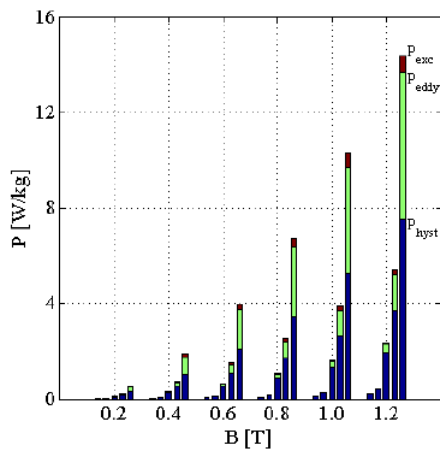


Fig. 11. Loss components at 20°C

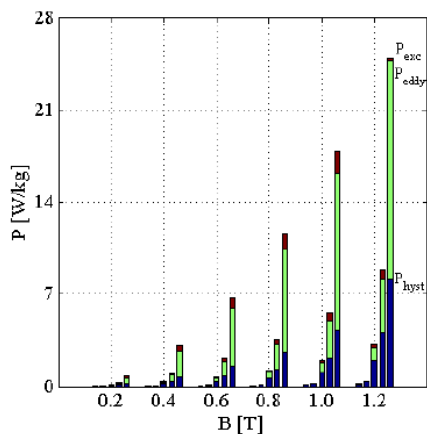


Fig. 12. Loss components at 420°C

Conclusion

The scalar Preisach model of hysteresis has been extended to take frequency as well as temperature into account simultaneously. The static term of the magnetic field intensity can be realized by other hysteresis models, too. Aim of further research is to apply the Jiles–Atherton model.

An important observation is highlighted. The hysteresis characteristics at about 100°C and at the room temperature are more or less the same. It is very important to check, because this is the typical temperature inside an electric motor. It is noted that the developed model is planned to extend the simulation of vector hysteresis properties, however the measurement of such phenomena inside a chamber is extremely difficult to realize.

The model is planned to insert into finite element simulations, especially to model and design electric motors.

Acknowledgement

Supported by the ÚNKP-17-4 New National Excellence Program of the Ministry of Human Capacities.

The Author thanks to István Drotár, Péter Prukner, Prof. Ibolya Zsoldos, Dr. Gábor Dogossy and László Varga the support during preparing the measurements.

Authors: Prof. M. Kuczmann, Department of Automation, Faculty of Mechanical Engineering, Informatics and Electrical Engineering, Széchenyi István University, Egyetem tér 1, H9026, Győr, Hungary, email: kuczmann@sze.hu.

REFERENCES

- [1] Ladjimi A., Mékideche M. R.: Modeling of Thermal Effects on Magnetic Hysteresis using the Jiles–Atherton Model, *Przeglad Elektrotechniczny*, 88(4a), pp. 253–256, 2012.
- [2] Cardelli A.: Modelling of Ferromagnetic Hysteresis in Soft Magnetic Materials, *Przeglad Elektrotechniczny*, 10, pp. 693–701, 2003. Fig. 12. Loss components at 420_C
- [3] Walecki K., Zakrzewski K.: The Total Iron Loss Determination in the Ferromagnetic Elements of the Electromagnetic Speed and Torque Converter Including the Magnetization Type, *Przeglad Elektrotechniczny*, 07a, pp. no. 201, 2012.
- [4] Pluta W.: Calculating power loss in electrical steel taking into account magnetic anisotropy, *Przeglad Elektrotechniczny*, 02, pp. no. 100, 2018.
- [5] Pardavi-Horvath M., Vertesy G.: Temperature Dependence of Switching Properties of a 2-D Array of Preisach-Type Particles, *IEEE Trans. on Magnetics*, 31(6), pp. 2910–2912, 1995.
- [6] Adly A. A., Mayergoz I. D.: Simulation of Field-Temperature Effects in Magnetic Media Using Anisotropic Preisach Models, *IEEE Trans. on Magnetics*, 34(4), pp. 1264–1266, 1998.
- [7] Nakmahachalasint P., Khai D. T., Loc V.-Q.: Thermal Behavior of a Dynamic Domain-Wall Motion Model for Hysteresis in Power Ferrite, *IEEE Trans. on Magnetics*, 41(1), pp. 140–143, 2005.
- [8] Lu H. Y., Zhu J. G., Ron-Hui S. Y.: Measurement and Modeling of Thermal Effects on Magnetic Hysteresis of Soft Ferrites, *IEEE Trans. on Magnetics*, 43(11), pp. 3952–3960, 2007.
- [9] Raghunathan A., Melikhov Y., Snyder J. E., Jiles D. C.: Modeling the Temperature Dependence of Hysteresis Based on Jiles–Atherton Theory, *IEEE Trans. on Magnetics*, 45(10), pp. 3954–3957, 2009.
- [10] Takahashi N., Morishita M., Miyagi D., Nakano N.: Examination of Magnetic Properties of Magnetic Materials at High Temperature Using a Ring Specimen, *IEEE Trans. on Magnetics*, 46(2), pp. 548–551, 2010.
- [11] Raghunathan A., Melikhov Y., Snyder J. E., Jiles D. C.: Theoretical Model of Temperature Dependence of Hysteresis Based on Mean Field Theory, *IEEE Trans. on Magnetics*, 46(6), pp. 1507–1510, 2010.
- [12] Hilal A., Raulet M. A., Martin C.: Magnetic Components Dynamic Modeling with Thermal Coupling for Circuit Simulators, *IEEE Trans. on Magnetics*, 50(4), 7026604, 2014.
- [13] Kuczmann M.: Fourier Transform and Controlling of Flux in Scalar Hysteresis Measurement, *Physica B*, 403(2-3), pp. 410–413, 2008.
- [14] Kis P., Kuczmann M., Fűzi J., Iványi A.: Hysteresis Measurement in LabVIEW, *Physica B*, 343(1-4), pp. 357–363, 2004.
- [15] Iványi A.: Hysteresis Models in Electromagnetic Computation, Academic Press, Budapest, 2017.
- [16] Zirka S. E., Moroz Y. I., Moses A. J., Arturi C. M.: Static and Dynamic Hysteresis Models for Studying Transformer Transients, *IEEE Trans. on Power Delivery*, 26(4), pp. 2352–2362, 2011.
- [17] Zirka S. E., Moroz Y. I., Moses A. J., Arturi C. M.: Viscous-Type Dynamic Hysteresis Model as a Tool for Loss Separation in Conducting Ferromagnetic Laminations, *IEEE Trans. on Magnetics*, 41(3), pp. 1109–1111, 2005.
- [18] Dlala E.: Comparison of models for estimating magnetic core losses in electrical machines using the finite element method, *IEEE Trans. on Magnetics*, 45(2), pp. 716–725, 2009.
- [19] Dlala E., Belahcen A., Arkkio A.: Magnetodynamic vector hysteresis model of ferromagnetic steel laminations, *Physica B*, 403, pp. 428–432, 2008.